# Effect of electrolyte temperature on the formation of self-organized anodic niobium oxide microcones in hot phosphate-glycerol electrolyte

S. Yang, Y. Aoki and H. Habazaki*

[1] Division of Materials Chemistry, Faculty of Engineering, Hokkaido University, Sapporo 060-8628, Japan

*Corresponding author; phone & fax: +81-11-706-6575, e-mail: habazaki@eng.hokudai.ac.jp

**Abstract**

Nanoporous niobium oxide films with microcone-type surface morphology were formed by anodizing at 10 V in glycerol electrolyte containing 0.6 mol $dm^{-3}$ $K_2HPO_4$ and 0.2 mol $dm^{-3}$ $K_3PO_4$ in a temperature range of 428-453 K. The microcones appeared after prolonged anodizing, but the required time was largely reduced by increasing electrolyte temperature. The anodic oxide was initially amorphous at all temperatures, but crystalline oxide nucleated during anodizing. The anodic oxide microcones, which were crystalline, appeared on surface as a consequence of preferential chemical dissolution of initially formed amorphous oxide. The chemical dissolution of an initially formed amorphous layer was accelerated by increasing the electrolyte temperature, with negligible influence of the temperature on the morphology of microcones up to 448 K.

Keywords: anodizing, anodic oxide, nanoporous film, self-organization, organic electrolyte

## 1. Introduction

Metal oxides of controlled micro-/nano-morphologies have received increased attention due to their promising properties and applications, such as catalysis, sensors, solar energy conversion and superhydrophobicity. Anodizing of metals is one of the cost-effective means for producing nano-structured metal oxide films on a range of metals and alloys. A nanoporous anodic alumina film with a hexagonal pore array [1, 2] is a well-

known example of self-organized materials, and the alumina films are of great interest as templates for the preparation of various nanofibers and nanotubes [3, 4] and as nano-devices [5-7]. In the last decade, nanotubular, nanofibrous and nanoporous anodic oxide films have also been fabricated on a range of metals, including iron [8], niobium [9, 10], titanium [11], tantalum [12], tungsten [13] and zirconium [14].

Except for the alumina films, the nanoporous and nanotubular anodic films are usually formed in fluoride-containing aqueous and organic electrolytes. The anodic films are usually amorphous and highly contaminated with fluoride species. Hot phosphate-containing glycerol electrolyte is another interesting electrolyte, in which nanoporous anodic oxide films can be formed on aluminum, titanium and its alloys, niobium and tantalum in phosphate-containing glycerol electrolytes at elevated temperatures [15-21]. In this electrolyte, incorporation of electrolyte species is suppressed, such that relatively pure metal oxide nanoporous films are formed.

When niobium was anodized in the glycerol electrolyte containing $K_2HPO_4$ and $K_3PO_4$ at 433 K, unique nanoporous oxide films with microcone-type surface morphology were developed [19]. The microcones appeared on the surface only after prolonged anodizing, indicating that the microcones were disclosed as a consequence of preferential dissolution of an initially formed oxide layer. From XRD patterns of the anodized specimens, the microcones consisted of crystalline $Nb_2O_5$. The formation of crystalline anodic niobium oxide microcones were also reported in fluoride-containing aqueous electrolytes [22-24]. The microcones of niobium oxide may have many interesting

potential applications. As one of examples, superhydrophilic properties and superhydrophobic properties after surface coating with fluoroalkylsilane have already been demonstrated using the microcones [19].

For the application of the anodic niobium oxide microcones, controlling the morphology of the porous oxide films is of crucial importance. In this work, we examined the influence of electrolyte temperature on growth and morphology of niobium oxide microcones. We found negligible influence of the temperature on the morphology of niobium oxide microcones, but the formation of microcones was highly accelerated by increasing the electrolyte temperature.

## 2. Experimental details

The specimens used for anodizing were cut from 99.9% niobium sheet, of 0.2 mm thickness; individual specimens were ultrasonically degreased in acetone. The electrolyte employed for anodizing was 0.6 mol $dm^{-3}$ $K_2HPO_4$ + 0.2 mol $dm^{-3}$ $K_3PO_4$ in glycerol at temperatures ranging from 428 to 453 K. The specimens were anodized at a constant current density of 250 A $m^{-2}$ to 10 V, followed by holding at 10 V for various durations. A two-electrode cell with a platinum counter electrode was used for anodizing. In some cases, the anodized specimens were kept in the electrolyte for selected periods of time without applying voltage. The anodizing and immersion were carried out under a dry nitrogen atmosphere to avoid incorporation of water into the electrolyte from humid air. The water content, measured by a Karl-Fisher titration method before anodizing, was 0.25 mass%.

After anodizing, the surfaces and cross-sections of the specimens were observed in a JEOL JSM-6500F field emission gun scanning electron microscope. The structures of the anodic films were analyzed by a Rigaku, RINT-2000 X-ray diffractometer using Cu Kα radiation under a θ-2θ mode.

## 3. Experimental Results

### 3.1. Voltage-time and current-time responses

Figure 1 shows the voltage-time and current-time curves of niobium during anodizing at 10 V, following initial galvanostatic anodizing at 250 A $m^{-2}$, in 0.6 mol $dm^{-3}$ $K_2HPO_4$-0.2 mol $dm^{-3}$ $K_3PO_4$-glycerol electrolyte containing 0.25 mass% water at different temperatures. During the initial constant current anodizing, the cell voltage is 4.6-5.0 V at 433 K, and then a sharp voltage rise to 10 V occurs at anodizing time of ~65 s. The sharp voltage rise is delayed to ~195 s and ~340 s by increasing the electrolyte temperature to 443 K and 453 K, respectively, while the cell voltage during the initial constant current anodizing decreases to 3.9-4.5 V and 3.3-4.2 V.

After reaching 10 V, an abrupt current decrease occurs at all three temperatures. However, current rise commences again at 453 K, and a current peak of 250 A $m^{-2}$ appears before a continuous current decrease proceeds. The current increase becomes less significant at lower temperatures, and the current peak changes to a current shoulder at 433 K. However, the anodizing time necessary to obtain the current peak or shoulder, which is ~900 s, is not dependent upon the temperature.

### 3.2. Phases in anodic oxides

Figure 2 shows X-ray diffraction patterns of niobium after anodizing for 5.4 ks at temperatures ranging from 428 to 453 K. Peaks of crystalline $Nb_2O_5$ exist at all temperatures in addition to peaks originating from niobium substrate. Halo patterns are also visible at diffraction angles centering ~28° and 58° at 428 K, suggesting the presence of amorphous oxide. The halo becomes weak with an increase in temperature, such that the crystalline oxide becomes a major phase at higher temperatures.

In order to examine the crystallization behavior of the anodic oxide films, X-ray diffraction patterns were measured after different periods of anodizing (Fig. 3). At all temperatures of 433, 443 and 453 K, the peaks of crystalline $Nb_2O_5$ detected after anodizing for 500-720 s increase during further anodizing. The results suggest that the initially formed anodic oxide is amorphous, and the crystalline oxide develops when the current increase commences (Fig. 1) at all temperatures.

### 3.3. Morphology of anodic oxide films

Figure 4 shows the change in the surface morphology with anodizing time at the temperature of 443 K. After anodizing for 1.8 ks, a nanoporous anodic oxide film is developed with no microcone morphology. The microcones of anodic oxide, consisting of nanofibrous oxide, appear after anodizing for 3.6 ks, although parts of microcones are covered with non-fibrous materials. The non-fibrous materials, which should be initially formed amorphous oxide, dissolve completely after anodizing for 5.4 ks, and only nanofibrous microcones are present on the surface. In contrast, no microcones appear even

after anodizing for 5.4 ks at a lower temperature of 433 K (Fig. 5a), although, from the XRD pattern (Fig. 2), crystalline oxide is developed. The absence of microcones on the film surface may be due to the presence of initially formed amorphous oxide at the outer part of anodic oxide film, which covers the crystalline microcones. To dissolve the amorphous oxide, the specimens anodized for 5.4 ks at 433 K were further simply immersed in the electrolyte at the same temperature for 1.8 ks (Fig. 5b) and 3.6 ks (Fig. 5c). The microcones appear partly after immersion for 1.8 ks and completely after immersion for 3.6 ks. When the same anodized specimen was immersed in the electrolyte at a higher temperature of 443 K, the dissolution rate of amorphous layer was enhanced and microcones were fully disclosed on surface after immersion only for 1.8 ks (Fig. 5d).

The changes in the surface morphology with anodizing temperature, anodizing time and subsequent immersion in electrolyte are summarized in Fig. 6. The necessary anodizing time to disclose microcones is only 2.7 ks at 453 K, but increases to 5.4 ks at 443 K. No microcones appear on film surface below 443 K even after anodizing for 5.4 ks, due to slow chemical dissolution of initially formed amorphous oxide. Additional immersion in the electrolyte discloses the microcones on the film surface. The total anodizing and immersion time necessary to see microcones at 428 K is 11.4 ks, which is more than 4 times that at 453 K. In contrast to the marked change in the anodizing and immersion time for fabrication of microcones, the morphology of microcones is little influenced by the temperature of anodizing. The sizes of the microcones are similar at all temperatures examined and in a range of 5 to 20 μm in size. Cross-sectional images (Fig. 7) also disclose the similar morphology of microcones formed at different temperatures. All the microcones

consist of highly branched nanofibers of niobium oxide, as seen in high magnification SEM image shown in Fig. 8a. The nanofibrous structure is also obvious from a cross-sectional SEM image shown in Fig. 8b.

The microcones should be formed as a consequence of preferential chemical dissolution of initially formed amorphous nanoporous oxide layer. However, crystalline microcones themselves suffer from chemical dissolution. Prolonged anodizing or immersion after disclosing microcones on surface changes their morphology (Fig. 6). Nanofibers disappear after longer anodizing and/or immersion at and above 443 K, and crack-like features of micrometer size are found in individual microcones and at boundaries of neighboring microcones. Thus, crystalline niobium oxide is also not so highly stable in the electrolyte at elevated temperatures, although the dissolution rate should be lower than that of the respective amorphous oxide.

## 4. Discussion

The present study revealed the formation of anodic niobium oxide microcones in phosphate-glycerol electrolyte at temperatures ranging from 428 K to 453 K. The microcones consist of highly branched nanofibrous oxide, which should be crystalline $Nb_2O_5$. The crystalline oxide seems to nucleate at anodizing time of 500-750 s, during which the current rises at all temperatures examined. The current rise is more significant at higher temperatures, suggesting faster growth of crystalline oxide. However, similar morphology of microcones at all temperatures indicates that the nucleation density of microcones is little dependent upon anodizing temperature. The microcones appear on the

surface after certain times of anodizing. At lower temperatures, additional immersion in the electrolyte is necessary after anodizing for 5.4 ks to disclose microcones. An amorphous niobium oxide layer is formed during initial anodizing before nucleation of crystalline oxide. After chemical dissolution of initially formed amorphous oxide, crystalline oxide microcones appear on the film surface [19]. Due to accelerated chemical dissolution at higher temperatures, microcones are visible at shorter anodizing time or shorter immersion time by increasing temperature, although chemical dissolution of crystalline oxide is also not negligible at least at and above 443 K (Fig. 6).

It is known that crystallization of anodic niobium oxide proceeds during formation of nonporous-type, so called barrier-type anodic oxide films in aqueous electrolytes [25-30]. Even for the barrier-type anodic oxide films, the initially formed anodic oxide films are amorphous, and crystalline oxide nucleates during anodizing. The crystallization is accelerated by increasing the formation voltage and anodizing temperature [26]. It has been proposed that an air-formed oxide, which is present before anodizing, becomes a nucleation site of crystalline oxide [30]. However, that is not the case of the present porous anodic oxide film, since the thin air-formed film should dissolve chemically before nucleation. Electrolyte species, generally incorporated into the barrier-type anodic oxide films formed at ambient temperature, impede the nucleation of crystalline oxide [30-32]. Higher amounts of electrolyte species are generally incorporated at lower temperatures [33, 34]. In contrast, negligible incorporation of phosphate has been reported in the anodic niobium oxide films formed in hot phosphate-glycerol electrolyte [16]. The formation of relatively pure $Nb_2O_5$

with little phosphate incorporation at all temperatures may be one of the reasons for the formation of similar morphology of microcones at all temperatures.

## 5. Conclusions

Self-organized nanoporous anodic oxide films with microcone-type surface morphology of 5-20 μm in size are fabricated by anodizing at 10 V in glycerol electrolyte containing 0.6 mol $dm^{-3}$ $K_2HPO_4$ and 0.2 mol $dm^{-3}$ $K_3PO_4$ at temperatures ranging from 428 to 453 K. The size and morphology of the microcones, which consist of highly branched nanofibrous crystalline $Nb_2O_5$, are not influenced by the anodizing temperature, but microcones appear on the film surface at shorter anodizing time, mainly due to accelerated chemical dissolution of initially formed amorphous oxide at higher temperatures. Anodizing for as short as 2.7 ks discloses microcones at 453 K. The crystalline oxide also suffers from chemical dissolution at least at and above 443 K, such that there is an appropriate anodizing time to form unique highly branched nanofibrous microcones of niobium oxide at each temperature.

**Acknowledgement**

The present work was supported in part by Grant-in-Aid for Exploratory Research, No.21656180 from the Japan Society for the Promotion of Science, and also by the Global COE Program (Project No. B01: Catalysis as the Basis for Innovation in Materials Science) from the Ministry of Education, Culture, Sports, Science and Technology, Japan.

**References**

[1] F. Keller, M.S. Hunter, D.L. Robinson, Structural features of oxide coatings on aluminum, J. Electrochem. Soc., 100 (1953) 411.

[2] J.P. O'Sullivan, G.C. Wood, Morphology and mechanism of formation of porous anodic films on aluminum, Proc. R. Soc. London, A, 317 (1970) 511-543.

[3] C.R. Martin, Nanomaterials - a membrane-based synthetic approach, Science, 266 (1994) 1961-1966.

[4] C.R. Martin, Membrane-based synthesis of nanomaterials, Chem. Mater., 8 (1996) 1739-1746.

[5] H. Masuda, K. Fukuda, Ordered metal nanohole arrays made by a 2-step replication of honeycomb structures of anodic alumina, Science, 268 (1995) 1466-1468.

[6] H. Masuda, M. Ohya, H. Asoh, M. Nakao, M. Nohtomi, T. Tamamura, Photonic crystal using anodic porous alumina, Jpn. J. Appl. Phys., Part 2-Let., 38 (1999) L1403-L1405.

[7] F. Matsumoto, K. Nishio, H. Masuda, Flow-through-type DNA array based on ideally ordered anodic porous alumina substrate, Adv. Mater., 16 (2004) 2105-2108.

[8] H.E. Prakasam, O.K. Varghese, M. Paulose, G.K. Mor, C.A. Grimes, Synthesis and photoelectrochemical properties of nanoporous iron (iii) oxide by potentiostatic anodization, Nanotechnol., 17 (2006) 4285-4291.

[9] A. Mozalev, M. Sakairi, I. Saeki, H. Takahashi, Nucleation and growth of the nanostructured anodic oxides on tantalum and niobium under the porous alumina film, Electrochim. Acta, 48 (2003) 3155-3170.

[10] I. Sieber, H. Hildebrand, A. Friedrich, P. Schmuki, Formation of self-organized niobium porous oxide on niobium, Electrochem. Commun., 7 (2005) 97-100.

[11] V. Zwilling, E. Darque-Ceretti, A. Boutry-Forveille, D. David, M.Y. Perrin, M. Aucouturier, Structure and physicochemistry of anodic oxide films on titanium and TA6V alloy, Surf. Interface Anal., 27 (1999) 629-637.

[12] I. Sieber, B. Kannan, P. Schmuki, Self-assembled porous tantalum oxide prepared in $H_2SO_4$/HF electrolytes, Electrochem. Solid State Let., 8 (2005) J10-J12.

[13] H. Tsuchiya, J.M. Macak, I. Sieber, L. Taveira, A. Ghicov, K. Sirotna, P. Schmuki, Self-organized porous $WO_3$ formed in NaF electrolytes, Electrochem. Commun., 7 (2005) 295-298.

[14] H. Tsuchiya, P. Schmuki, Thick self-organized porous zirconium oxide formed in $H_2SO_4$/$NH_4F$ electrolytes, Electrochem. Commun., 6 (2004) 1131-1134.

[15] Q. Lu, G. Alcala, P. Skeldon, G.E. Thompson, M.J. Graham, D. Masheder, K. Shimizu, H. Habazaki, Porous tantala and alumina films from non-thickness limited anodising in phosphate/glycerol electrolyte, Electrochim. Acta, 48 (2002) 37-42.

[16] Q. Lu, T. Hashimoto, P. Skeldon, G.E. Thompson, H. Habazaki, K. Shimizu, Nanoporous anodic niobium oxide formed in phosphate/glycerol electrolyte, Electrochem. Solid State Let., 8 (2005) B17-B20.

[17] H. Habazaki, Y. Oikawa, K. Fushimi, Y. Aoki, K. Shimizu, P. Skeldon, G.E. Thompson, Importance of water content in formation of porous anodic niobium oxide films in hot phosphate-glycerol electrolyte, Electrochim. Acta, 54 (2009) 946-951.

[18] H. Habazaki, Y. Oikawa, K. Fushimi, K. Shimizu, S. Nagata, P. Skeldon, G.E. Thompson, Formation of porous anodic films on Ti-Si alloys in hot phosphate-glycerol electrolyte, Electrochim. Acta, 53 (2007) 1775-1781.

[19] Y. Oikawa, T. Minami, H. Mayama, K. Tsujii, K. Fushimi, Y. Aoki, P. Skeldon, G.E. Thompson, H. Habazaki, Preparation of self-organized porous anodic niobium oxide microcones and their surface wettability, Acta Mater., 57 (2009) 3941-3946.

[20] H. Habazaki, M. Teraoka, Y. Aoki, P. Skeldon, G.E. Thompson, Formation of porous anodic titanium oxide films in hot phosphate/glycerol electrolyte, Electrochim. Acta, 55 (2010) 3939-3943.

[21] K. Lee, D. Kim, P. Roy, I. Paramasivam, B.I. Birajdar, E. Spiecker, P. Schmuki, Anodic formation of thick anatase $TiO_2$ mesosponge layers for high-efficiency photocatalysis, J. Am. Chem. Soc., 132 (2010) 1478-1480.

[22] R.L. Karlinsey, Preparation of self-organized niobium oxide microstructures via potentiostatic anodization, Electrochem. Commun., 7 (2005) 1190-1194.

[23] R.L. Karlinsey, Self-assembled $Nb_2O_5$ microcones with tailored crystallinity, J. Mater. Sci., 41 (2006) 5017-5020.

[24] J.L. Zhao, X.X. Wang, R.Q. Xu, Y.J. Mi, Y.X. Li, Preparation and growth mechanism of niobium oxide microcones by the anodization method, Electrochem. Solid State Let., 10 (2007) C31-C33.

[25] D.M. Lakhiani, L.L. Shreir, Crystallization of amorphous Nb oxide during anodic oxidation, Nature, 188 (1960) 49-50.

[26] N.F. Jackson, J.C. Hendy, Use of niobium as an anode material in liquid filled electrolytic capacitors, Electrocomponent Science and Technology, 1 (1974) 27-37.

[27] H. Asoh, H. Odate, S. Ono, Crystallization and dielectric properties of anodic oxide films formed on niobium, J. Surf. FInish. Soc. Jpn., 55 (2004) 952-959.

[28] K. Nagahara, M. Sakairi, H. Takahashi, K. Matsumoto, K. Takayama, Y. Oda, Change in the structure and dielectric properties of niobium anodic oxide films during potentiostatic anodizing, Elechem., 72 (2004) 624-632.

[29] K. Nagahara, M. Sakairi, H. Takahashi, K. Matsumoto, K. Takayama, Y. Oda, Mechanism of formation and growth of sunflower-shaped imperfections in anodic oxide films on niobium, Electrochim. Acta, 52 (2007) 2134-2145.

[30] H. Habazaki, T. Ogasawara, H. Konno, K. Shimizu, S. Nagata, P. Skeldon, G.E. Thompson, Field crystallization of anodic niobia, Corros. Sci., 49 (2007) 580-593.

[31] K. Shimizu, G.E. Thompson, G.C. Wood, Direct observation of the duplex nature of anodic barrier films on aluminium, Thin Solid Films, 81 (1981) 39-44.

[32] K. Shimizu, G.E. Thompson, G.C. Wood, Electron-beam-induced crystallization of anodic barrier films on aluminium, Thin Solid Films, 77 (1981) 313-318.

[33] Q. Lu, P. Skeldon, G.E. Thompson, D. Masheder, H. Habazaki, K. Shimizu, Transport numbers of metal and oxygen species in anodic tantala, Corros. Sci., 46 (2004) 2817-2824.

[34] S. Ono, M. Baba, M. Shimoyama, H. Asoh, Structure and properties of anodic oxide films formed on niobium, in: V. Birss, L. Burke, A.R. Hillman, R.S. Lillard (Eds.) Surface Oxide Films, The Electrochemical Society, Orlando, 2004, pp. 133-142.

Figure captions

**Fig. 1** Current-time and voltage-time responses of niobium during anodizing at 10 V in glycerol electrolyte containing 0.6 mol $dm^{-3}$ $K_2HPO_4$ and 0.2 mol $dm^{-3}$ $K_3PO_4$ at 433, 443 and 453 K. Initially, a constant current density of 250 A $m^{-2}$ was applied before reaching 10 V.

**Fig. 2** X-ray diffraction patterns of niobium anodized at 10 V, following initial anodizing at 250 A $m^{-2}$ to 10 V, in glycerol electrolyte containing 0.6 mol $dm^{-3}$ $K_2HPO_4$ and 0.2 mol $dm^{-3}$ $K_3PO_4$ for 5.4 ks at several temperatures.

**Fig. 3** X-ray diffraction patterns of niobium anodized at 10 V, following initial anodizing at 250 A $m^{-2}$ to 10 V, in glycerol electrolyte containing 0.6 mol $dm^{-3}$ $K_2HPO_4$ and 0.2 mol $dm^{-3}$ $K_3PO_4$ for several periods of time at (a) 433 K, (b) 443 K and (c) 453 K.

**Fig. 4** Scanning electron micrographs of surfaces of niobium specimens anodized at 10 V, following initial anodizing at 250 A $m^{-2}$ to 10 V, in glycerol electrolyte containing 0.6 mol $dm^{-3}$ $K_2HPO_4$ and 0.2 mol $dm^{-3}$ $K_3PO_4$ for (a) 1.8 ks, (b) 3.6 ks and (c) 5.4 ks at 443 K.

**Fig. 5** Scanning electron micrographs of surfaces of niobium specimens anodized at 10 V, following initial anodizing at 250 A $m^{-2}$ to 10 V, in glycerol electrolyte containing 0.6 mol

$dm^{-3}$ $K_2HPO_4$ and 0.2 mol $dm^{-3}$ $K_3PO_4$ for 5.4 ks at 433 K and then immersed in the same electrolyte for (a) 0 s, (b) 1.8 ks and (c) 3.6 ks at 433 K and (d) for 1.8 ks at 443 K.

**Fig. 6** Change in the surface morphology of niobium specimens anodized at 10 V, following initial anodizing at 250 A $m^{-2}$ to 10 V, in glycerol electrolyte containing 0.6 mol $dm^{-3}$ $K_2HPO_4$ and 0.2 mol $dm^{-3}$ $K_3PO_4$ as a function of anodizing temperature, anodizing time and time of subsequent immersion.

**Fig. 7** Scanning electron micrographs of cross-sections of niobium specimens anodized at 10 V, following initial anodizing at 250 A $m^{-2}$ to 10 V, in glycerol electrolyte containing 0.6 mol $dm^{-3}$ $K_2HPO_4$ and 0.2 mol $dm^{-3}$ $K_3PO_4$ at (a) 433 K for 5.4 ks and immersing for 6.0 ks, (b) 443 K for 5.4 ks and (c) 453 K for 2.7 ks.

**Fig. 8** High magnification scanning electron micrograph of (a) surface and (b) cross-section of niobium anodized at 10 V, following initial anodizing at 250 A $m^{-2}$ to 10 V, in glycerol electrolyte containing 0.6 mol $dm^{-3}$ $K_2HPO_4$ and 0.2 mol $dm^{-3}$ $K_3PO_4$ at 443 K for 5.4 ks.

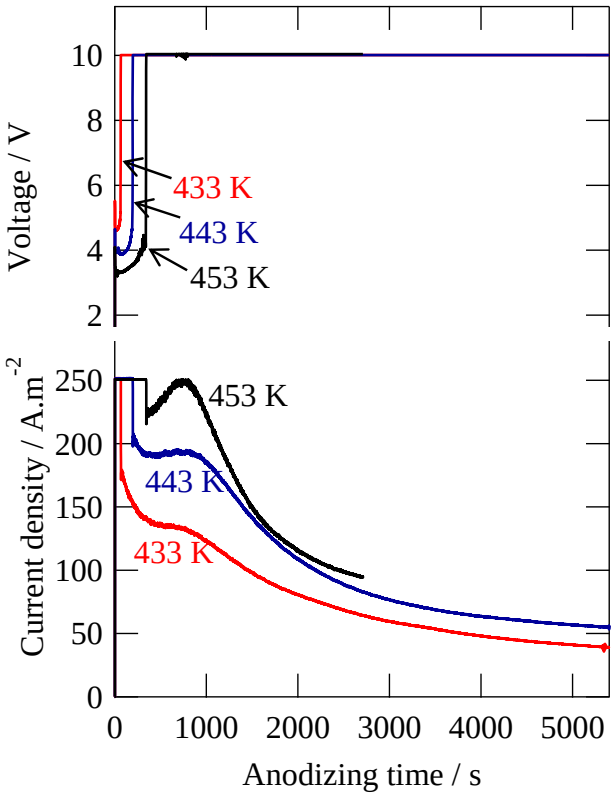


**Fig. 1** Current-time and voltage-time responses of niobium during anodizing at 10 V in glycerol electrolyte containing 0.6 mol $dm^{-3}$ $K_2HPO_4$ and 0.2 mol $dm^{-3}$ $K_3PO_4$ at 433, 443 and 453 K. Initially, a constant current density of 250 A $m^{-2}$ was applied before reaching 10 V.

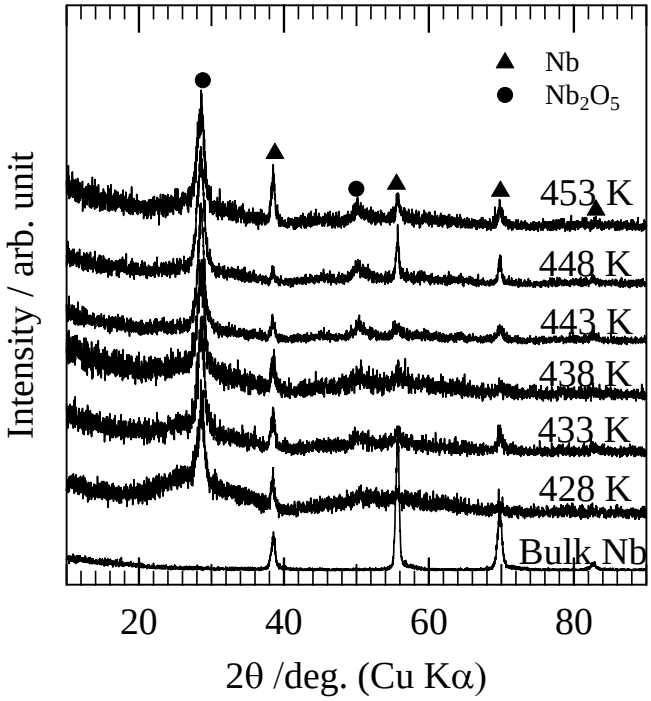


**Fig. 2** X-ray diffraction patterns of niobium anodized at 10 V, following initial anodizing at 250 A $m^{-2}$ to 10 V, in glycerol electrolyte containing 0.6 mol $dm^{-3}$ $K_2HPO_4$ and 0.2 mol $dm^{-3}$ $K_3PO_4$ for 5.4 ks at several temperatures.

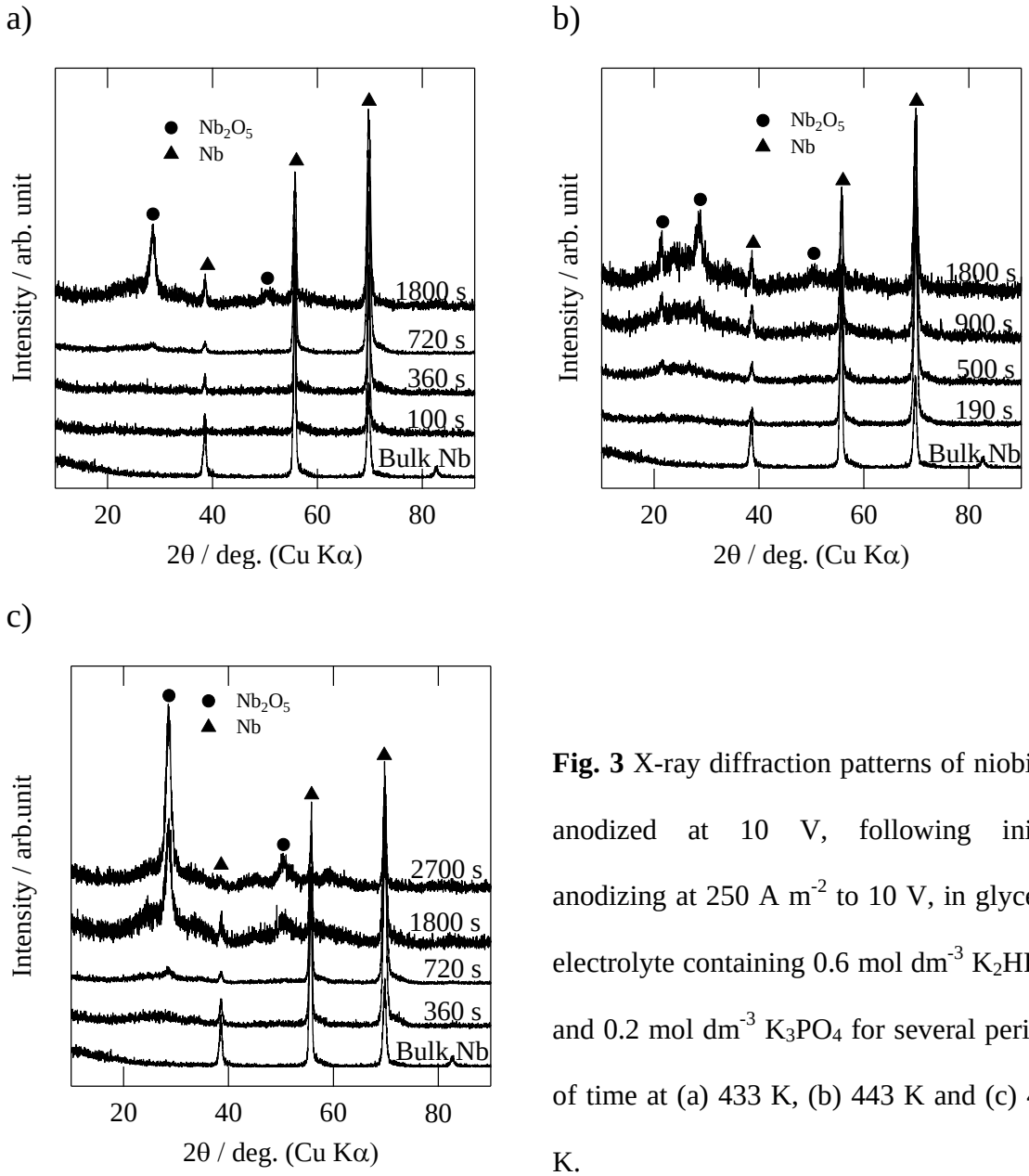


**Fig. 3** X-ray diffraction patterns of niobium anodized at 10 V, following initial anodizing at 250 A $m^{-2}$ to 10 V, in glycerol electrolyte containing 0.6 mol $dm^{-3}$ $K_2HPO_4$ and 0.2 mol $dm^{-3}$ $K_3PO_4$ for several periods of time at (a) 433 K, (b) 443 K and (c) 453 K.

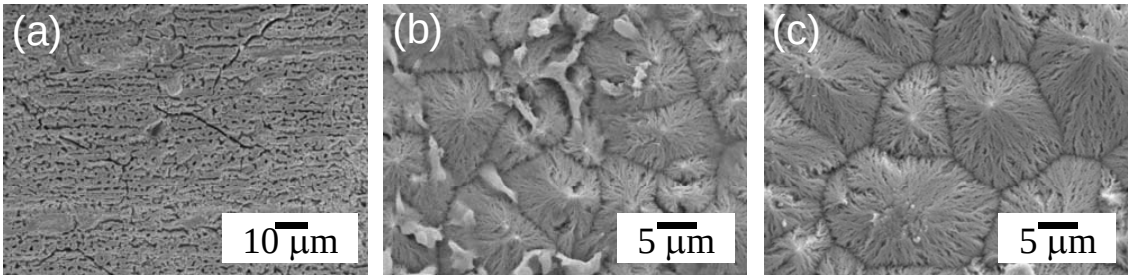


**Fig. 4** Scanning electron micrographs of surfaces of niobium specimens anodized at 10 V, following initial anodizing at 250 A $m^{-2}$ to 10 V, in glycerol electrolyte containing 0.6 mol $dm^{-3}$ $K_2HPO_4$ and 0.2 mol $dm^{-3}$ $K_3PO_4$ for (a) 1.8 ks, (b) 3.6 ks and (c) 5.4 ks at 443 K.

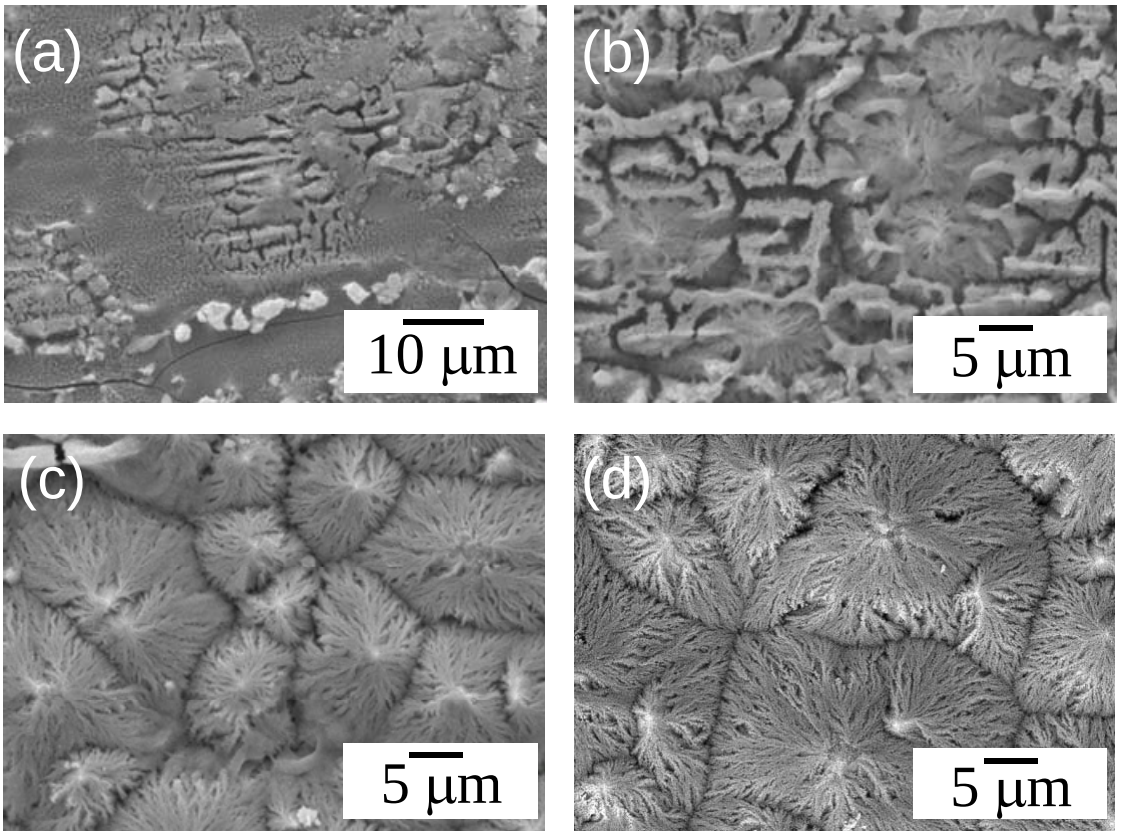


**Fig. 5** Scanning electron micrographs of surfaces of niobium specimens anodized at 10 V, following initial anodizing at 250 A $m^{-2}$ to 10 V, in glycerol electrolyte containing 0.6 mol $dm^{-3}$ $K_2HPO_4$ and 0.2 mol $dm^{-3}$ $K_3PO_4$ for 5.4 ks at 433 K and then immersed in the same electrolyte for (a) 0 s, (b) 1.8 ks and (c) 3.6 ks at 433 K and (d) for 1.8 ks at 443 K.

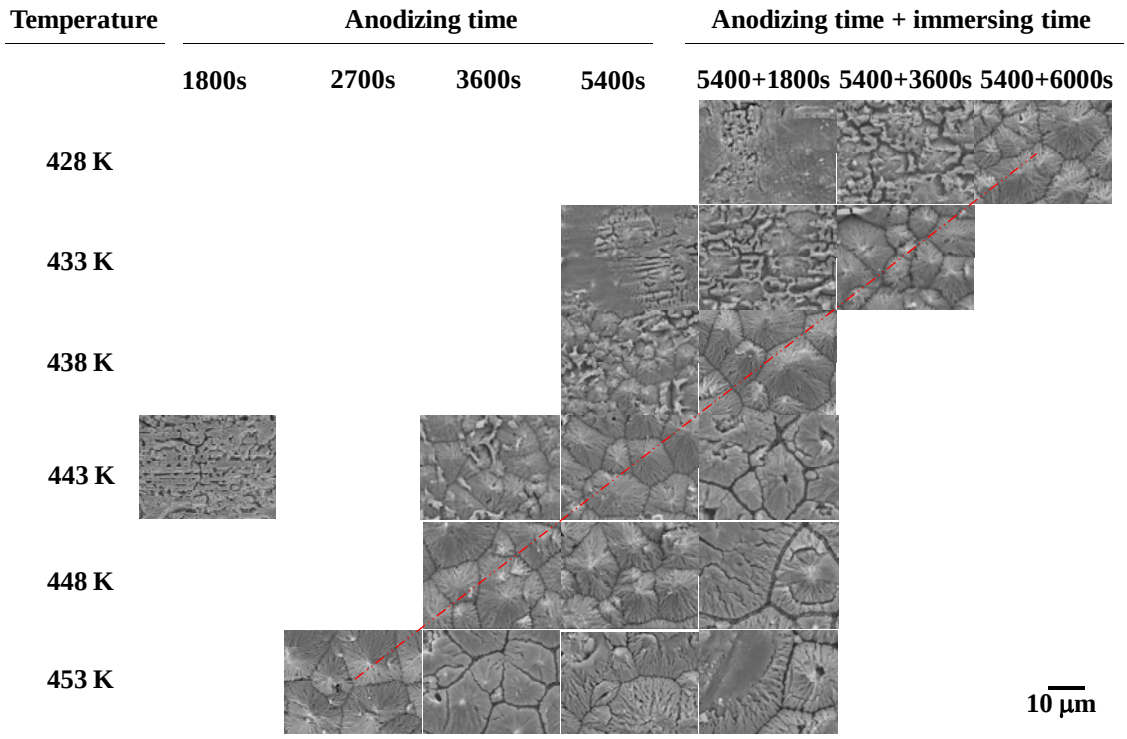


**Fig. 6** Change in the surface morphology of niobium specimens anodized at 10 V, following initial anodizing at 250 A $m^{-2}$ to 10 V, in glycerol electrolyte containing 0.6 mol $dm^{-3}$ $K_2HPO_4$ and 0.2 mol $dm^{-3}$ $K_3PO_4$ as a function of anodizing temperature, anodizing time and time of subsequent immersion.

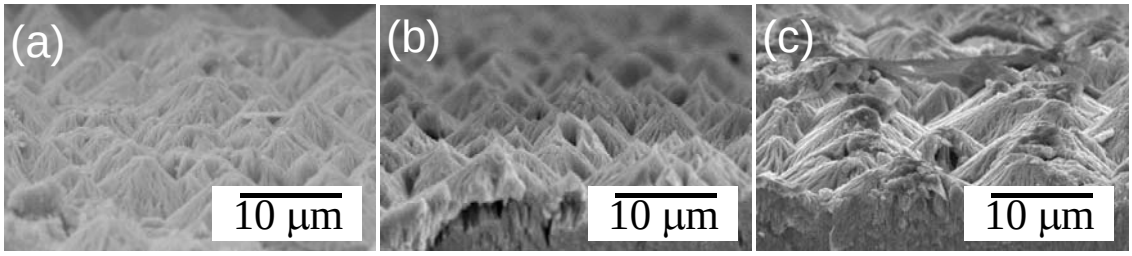


**Fig. 7** Scanning electron micrographs of cross-sections of niobium specimens anodized at 10 V, following initial anodizing at 250 A $m^{-2}$ to 10 V, in glycerol electrolyte containing 0.6 mol $dm^{-3}$ $K_2HPO_4$ and 0.2 mol $dm^{-3}$ $K_3PO_4$ at (a) 433 K for 5.4 ks and immersing for 6.0 ks, (b) 443 K for 5.4 ks and (c) 453 K for 2.7 ks.

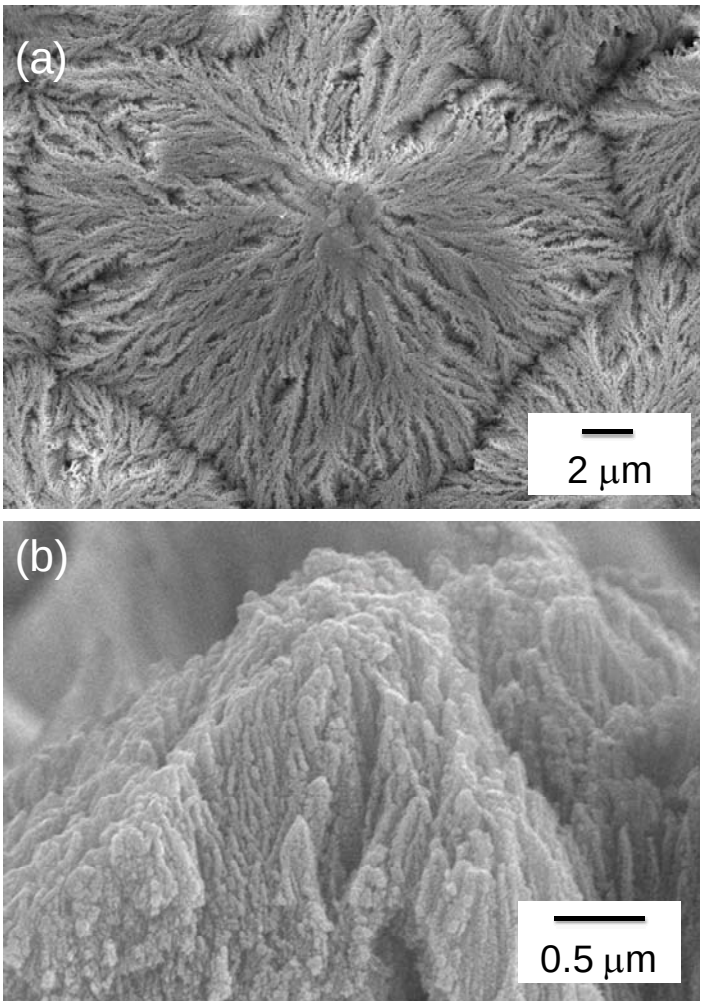


**Fig. 8** High magnification scanning electron micrograph of surface of niobium anodized at 10 V, following initial anodizing at 250 A $m^{-2}$ to 10 V, in glycerol electrolyte containing 0.6 mol $dm^{-3}$ $K_2HPO_4$ and 0.2 mol $dm^{-3}$ $K_3PO_4$ at 443 K for 5.4 ks.